Dual-band wide-angle scanning planar phased array in X/Ku-bands

Valavan, SE; Tran, DP; Yarovoy, A; Roederer, AG

DOI
10.1109/TAP.2014.2307336

Publication date
2014

Document Version
Accepted author manuscript

Published in
IEEE Transactions on Antennas and Propagation

Dual-Band Wide-Angle Scanning Planar Phased Array in X/Ku-Bands

S. E. Valavan, D. Tran, A. G. Yarovoy, *Senior Member, IEEE* and A. G. Roederer, *Life Fellow, IEEE*

***Abstract*— A novel planar dual-band phased array, operational in the X/Ku-bands and with wide-angle scanning capability is presented. The design, development and experimental demonstration are described. A new single-layer crossed L-bar microstrip antenna is used for the array design. The antenna has low-profile architecture, measuring only 0.33λ × 0.33λ, at the low frequency band of operation, with flexible resonance tuning capability offered by the use of a plate-through-hole and field-matching ring arrangement. A 49-element planar (7 × 7) array demonstrator has been built and its performance validated, exhibiting good agreement with full-wave simulations. The dual-band array supports a large frequency ratio of nearly 1.8:1, and also maintains good sub-band bandwidths. Wide-angle scanning up to a maximum of 60º and 50º are achieved at the low and high frequency bands of operation respectively.**

***Index Terms*— Phased arrays, multifrequency antennas, planar arrays, microstrip antennas.**

I. Introduction

The research on multifunction radars, with reconfigurable features, foreseen as the next generation of radar systems, has generated a huge volume of interest in both industry and academia [1-4]. Antenna array front-ends form a pivotal part of these radar systems. Enabling operation of several radar and communication functions, using the same aperture, are among the latest research trends in this domain. Antenna arrays covering two or more well-separated frequency bands (for example, X- and Ku-bands), with wide-angle scanning capabilities, can enable these systems to support different operational tasks in different bands and with the same aperture. A number of ultra-wideband antenna arrays have been proposed in the literature responding to such needs [5-7]. However, system demands would be better satisfied (e.g., in terms of vulnerability to external electromagnetic interferences) by multi-band antenna arrays with well separated operational sub-bands. Further, with the use of multi-band arrays, good isolation can be achieved between operations in different bands, which could possibly be allocated for implementing different target functions. A review of dual- or multi-band antennas proposed for array operations [8-15] reveals that most of these radiators suffer from one of four major performance limitations viz., very small frequency ratios between operational bands [10-11,15], large electrical dimensions [8, 10-11, 13,15], asymmetric or inconsistent radiation patterns [8-9] and/or absence of wide-angle impedance matching. The presence of one, or combination of these limitations, has often impeded successful developments of dual- or multi-band arrays.

In this paper, the design, development and experimental validation of a dual-band phased array supporting wide-angle scanning are presented. The proposed novel crossed L-bar antenna has been developed as an '*array-capable*' element with extremely low-profile electrical dimensions, measuring only $0.33\lambda_L \times 0.33\lambda_L$, at the low frequency band of operation. The simple single-layer geometry and the maintenance of dual-band impedance matching over wide scanning angles ($\pm 60^o$) in an infinite array are noteworthy characteristics of the dual-band array antenna. A planar 49-element (7 × 7) array of crossed L-bar antennas, optimised for performance in the X/Ku-bands, has been fabricated and its performance experimentally verified. The array supports dual-band operation with a maximum frequency ratio of nearly 1.8:1 between the bands. Wide-angle scanning up to a maximum of 60º and 50º are achieved at low and high frequency bands respectively. Furthermore, good bandwidths are also achieved in the operational bands.

The proposed dual-band microstrip antenna design provides new avenues to achieve 1) low-profile '*array-capable*' electrical dimensions, 2) large frequency ratio, 3) consistent radiation patterns and 4) wide-angle scanning capability. The remainder of the paper is organized as follows. The crossed L-bar antenna concept, design and its array performance are presented in Section II. The experimental results of the dual-band array demonstrator are summarised in Section III, followed by the conclusions in Section IV.

II. Dual-Band Antenna and Array Design

A. Crossed L-bar antenna concept and architecture

The basis of the proposed antenna concept can be explained as follows. Consider a radiating patch with a rectangular strip-like geometry, as shown in Fig. 1a. Exciting this patch by means of an off-centered feed can aid in supporting two operational modes, achieving dual-band operation. However, the length (L) of the patch needs to be large enough to

Manuscript received Sept 5, 2013; revised Nov 4, 2013; accepted Jan 28 2014. This research is conducted as part of the Sensor Technology Applied in Reconfigurable systems for sustainable Security (STARS) project. For further information: *www.starsproject.nl*.

S. E. Valavan, D. Tran, A. G. Yarovoy and A. G. Roederer are with MS3, Department of Electrical Engineering, Delft University of Technology, Mekelweg 4, 2628CD, Delft, Netherlands. (e-mail: s.e.amaldoss@tudelft.nl).

accommodate both the modes, which, in turn, would increase the electrical dimensions of the patch, especially at the high frequency band. Furthermore, for planar array implementations, it would be more attractive to have square unit-cells. The use of square unit-cells in arrays would help in maintaining similar inter-element spacing, along both the E- and H-planes of the radiator, whereby similar levels of scanning can be achieved along the principal planes.

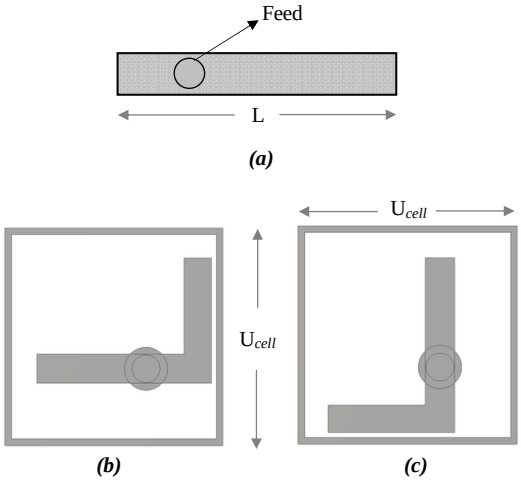

Fig. 1. (a) – Rectangular strip-like patch with off-centered feed, (b) – single L-bar geometry supporting vertical polarization, and (c) – single L-bar geometry supporting horizontal polarization. Square unit-cell used for illustration.

In order to accommodate the patch within a square unit-cell and still maintain dual-band operation, the strip-like patch is modified into an L-bar. Two possible configurations (supporting vertical or horizontal polarization) can be achieved, as shown in Figs. 1b-c. However, for both the designs, presented in Figs. 1b-c, the unit-cell would still be electrically large (> 0.6λ) at the high frequency band. These (electrically) large dimensions would negatively impact the scanning performance of the array at the operational bands. The crossed L-bar arrangement (Fig. 2a) is hence introduced to reduce the electrical dimensions of the unit-cell of the antenna. This is made possible by increasing the electrical size of the radiating aperture through the use of the crossed L-bar geometry. The resulting structure supports dual resonances at frequencies lower than the ones obtained with the single L-bar geometries. The approach is, in some manner, analogous to the use of meander line printed antenna geometries, which are often used to reduce the electrical dimensions of the respective patch antennas. The L-bar dimensions can be optimised to support dual-band operation and realize very small electrical dimensions of the unit-cell. The concept for achieving dual-band operation and low-profile electrical dimensions, with a simple single-layer geometry, is thus introduced.

The details of the other components of the antenna's unit-cell geometry are as follows. The feed pin of the SMA connector runs through the plate-through-hole (PTH) cylinder, which is placed in the substrate (Fig. 2b). A field matching ring is present at the junction (refer Fig. 2b) where the feed pin meets the crossed L-bars, at the top of the substrate. The diameter of the SMA feed pin dictates the inner diameter of both the plate-through-hole (PTH) cylinder, and the field matching ring. The entire assembly is enclosed within a cavity architecture, the dual functions of which are described in the latter part of this section. A dielectric substrate layer (with thickness 't') is used between the ground plane and the crossed L-bar patch (Fig. 2c).

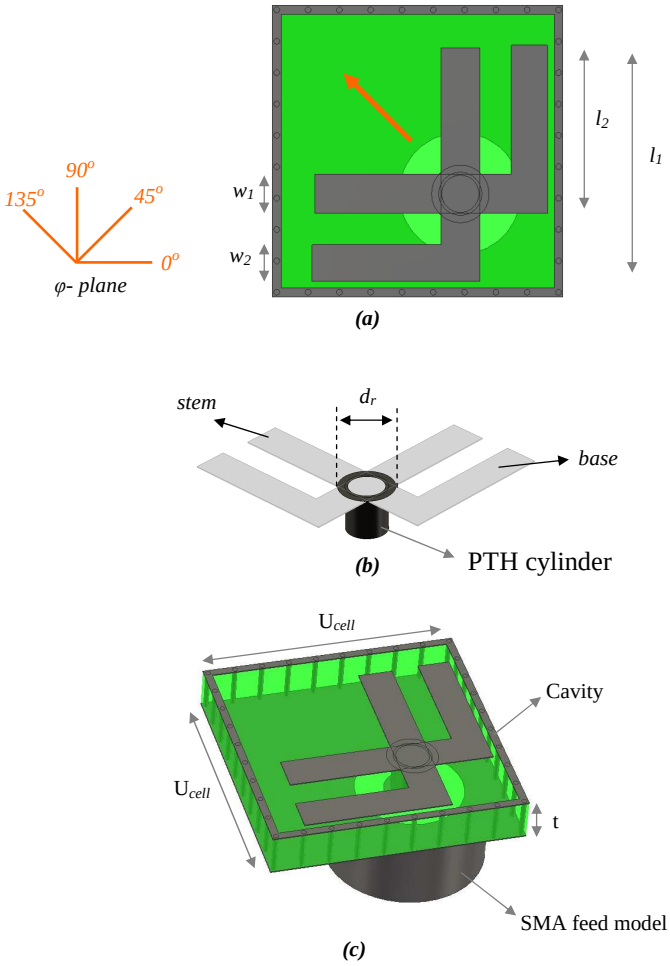

Fig. 2. Schematic of the proposed dual-band crossed L-bar antenna. (a) – top view, arrowhead denotes polarization, (b) – plate-through-hole (PTH) cylinder and matching-ring arrangement (feed apparatus), and (c) – perspective view, substrate maintained semi-transparent for illustration.

An important distinction, inherent to the design of the antenna, is with the polarization. The bases of the L-bars in conjunction with the respective sides of the cavity sustain orthogonal polarization components, resulting in waves polarized along the diagonal plane of the radiator (φ = 135° plane in Fig. 2a). Correspondingly, the E- and H-planes of the antenna are defined along the φ = 135° and φ = 45° planes respectively (refer to Fig. 2a). The cavity architecture, apart from its aforementioned role in the radiation mechanism, also helps in reducing coupling between elements, when implemented in arrays. A discussion on the antenna's mutual coupling characteristics is provided in Section II-B.

The computed current distribution plots of the stand-alone antenna, presented in Fig. 3, are used for illustrating the

radiation characteristics of the proposed dual-band antenna. The full-wave numerical modeling of the antenna was carried out in CST-MWS. Dielectric permittivity (ε_r) of 2.2 was used for the antenna's substrate (Rogers RT5880 [16]), and a characteristic impedance of 50Ω was maintained. The antenna supports dual-band operation with operational centre frequencies at 9.8 GHz and 17 GHz respectively.

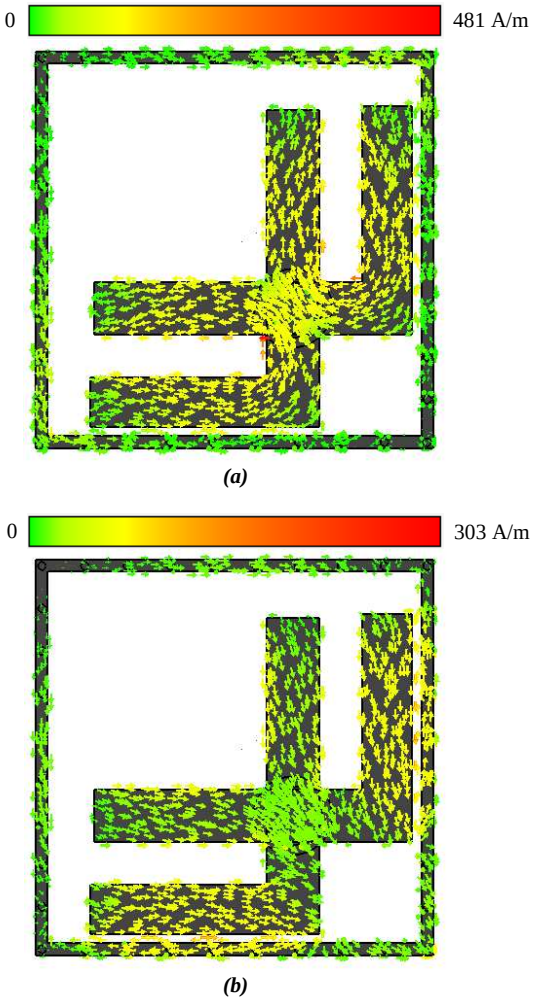

Fig. 3. Surface current distribution at the operational bands. (a)– 9.8 GHz (f_L) and (b)- 17 GHz (f_H).

The difference in the surface current distributions, as per the operational modes supported, is clearly illustrated in Fig. 3. It can also be noticed that at the low frequency band of operation (Fig. 3a), which requires larger electrical dimensions of the radiating part, the maximum amplitude of the surface currents, or the 'radiation spots', occurs along the stem (refer Fig. 2b) of the L-bars. The current path makes use of both the base and the stem of the L-bars at this low frequency band. On the other hand, the 'radiation spots' occur at the bases (refer to Fig. 2b) of the L-bars at the high frequency band (Fig. 3b). This difference in the radiation characteristics, at the operational bands, is also reiterated in the field distribution plots over the array, presented in Fig. 7. Furthermore, the presence of the orthogonal components and the role of the cavity in supporting these components, at both the operational bands, are also demonstrated through these plots (Fig. 3a-b).

The ratio of the lengths (l_1/l_2) and widths (w_1/w_2) of the L-bars were the main parameters used for the optimization of the antenna's performance in both infinite and finite-sized arrays. The variation of the widths' ratio controls the resonant band positions, whereas the lengths ratio aids in achieving the necessary impedance matching at the respective bands. The field matching-ring's outer diameter (d_r) provides an additional tuning parameter. This however, was maintained at 1.9 mm in the array optimization. Finally, it is worth noting that due to the use of identical L-bars, the variation in either or both the widths and lengths ratios would still maintain the structure to be symmetric along the diagonal plane (φ = 135° in Fig. 2a), leaving the orientation of the polarization unaffected.

The antenna concept presented can also be extended to support circular polarization in a target band, if required. This is achieved through the use of a modified grounded-pin technique, the details of which are presented in [17]. This technique however, is limited to stand-alone crossed L-bar antennas, which are not 'array-capable' and have larger (~0.7λ) unit-cell dimensions as well.

B. *Array performance*

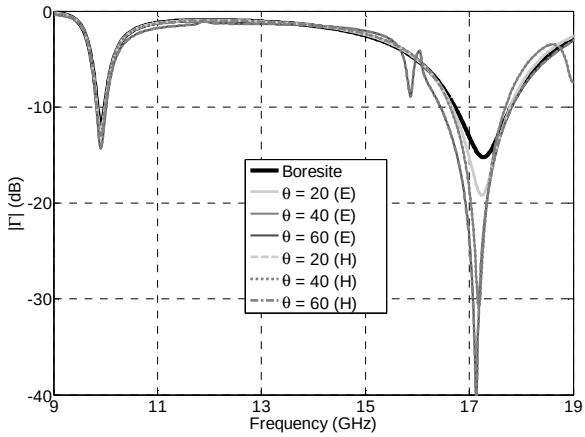

Fig. 4. Variation of active reflection coefficient ($|\Gamma_{act}|$) with scanning angle in infinite array.

Evaluation and optimization of the crossed L-bar antenna's performance in infinite array, using the frequency domain solver in CST-MWS, was carried out as the first step in the array analysis. The antenna's unit-cell dimension was maintained at 10.4 mm × 10.4 mm, which resulted in operational resonances in the X/Ku-bands (8 - 18 GHz). The variations of the dual-band characteristics and sub-band bandwidths with scanning angle were evaluated in the infinite array. The corresponding performance summary obtained with the infinite array simulation is presented in Fig. 4. The cavity architecture of the antenna helps in lowering the mutual coupling, thereby aiding to maintain the dual-band characteristics up to a maximum of 60° along both the principal planes of operation. Another key feature of the antenna's performance is the maintenance of the bandwidth at both the operational bands over wide scanning angles, with

only marginal variations at the high frequency band. This performance is significant and ensures the absence of any effects of scan blindness in the operational bands, up to a maximum 60° along the principal planes. The low-profile electrical dimensions of the unit-cell and the wide-angle impedance match characteristics of the dual-band antenna are both useful and advantageous for the array applications.

The development of finite-sized array forms an integral part of the array research for the verification of the proposed concepts. In this regard, the crossed L-bar antenna was implemented, and its performance optimised in a planar 7 × 7 array. The unit-cell of the antenna was further reduced to 10 mm × 10 mm, to improve the wide-angle scanning at the high frequency band. Retuning of the antenna's L-bar dimensions was hence required. The re-optimization procedure mainly involved the marginal retuning of the ratio of the L-bar lengths (l_1/l_2) and widths (w_1/w_2), maintaining a fixed diameter of the field matching ring (d_r=1.9 mm). The thickness (t) of the substrate was kept as per standard values available for fabrication [16]. The optimized element dimensions used in the planar array model are summarized in Table I.

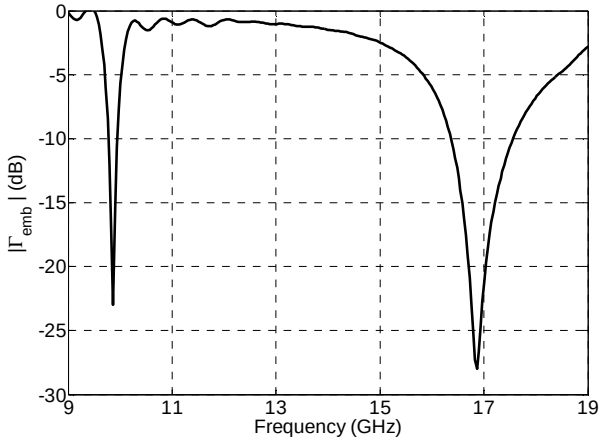

Fig. 5. Computed embedded input reflection coefficient (S_{2525}) of the centre element of the planar (7 × 7) array.

The computed embedded reflection coefficient of the centre element (no: 25) of the planar (7 × 7) array is shown in Fig. 5. The array supports well-defined sub-bands with a maximum frequency ratio of nearly 1.8:1. Bandwidths of 310 MHz and 1.2 GHz are achieved at the low and high frequency bands respectively. The corresponding embedded radiation patterns of the centre element at the operational centre frequencies are shown in Fig. 6. Consistent radiation patterns with cross polarization levels below -15 dB are achieved at both the bands. The broad characteristics of the embedded patterns, along both the principal planes, are well suited for wide-scan applications.

The dual-band array antenna's unit-cell (10 mm × 10 mm) measures only $0.33\lambda_L \times 0.33\lambda_L$ and $0.58\lambda_H \times 0.58\lambda_H$, at the low and high frequency bands of operation respectively. This low-profile size is vital, since it makes it possible to achieve grating-lobe-free scanning up to a maximum of 50° at the high frequency band of operation (16.2–17.4 GHz), as per the relation: $d_e = \lambda_{op} / 1 + \sin(\theta_{max})$. Where λ_{op} refers to the operational wavelength, d_e to the inter-element spacing and θ_{max} is the maximum possible grating-lobe-free scanning angle. The scanning performance of the planar dual-band array is covered in Section III.

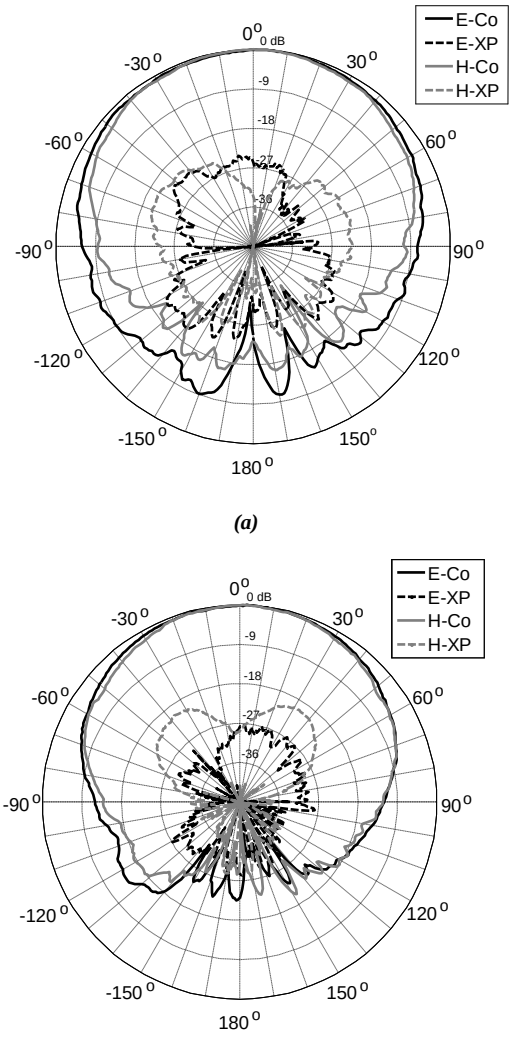

Fig. 6. Computed embedded radiation pattern of the centre element (no: 25) in planar array. (a)- 9.8 GHz and (b)- 17 GHz.

Finally, the effectiveness of the metal cavity to confine the field distribution within the unit-cell is demonstrated through the field distribution plots over the array, at the operational bands (Fig. 7). The plots are obtained by exciting the centre element (no: 25) of the array, with the other elements terminated in matched loads. It can be inferred that the field distribution is contained well within the unit-cell in both operational bands. Very low levels of coupling, below -30 dB, are obtained after the second adjacent element from the centre element. This behaviour is especially significant given the very small inter-element spacing (0.33λ) at the low frequency band. Furthermore, even the maximum levels of coupling, between the first adjacent radiator pairs (for example, between elements no: 25 and 26), in the low frequency band, are as low as -19.1

dB and -21.5 dB, along the E- and H-planes respectively.

The broad embedded radiation patterns and electrically small unit-cell dimensions, guarantee wide-angle grating-lobe-free scanning capability, while the low mutual coupling characteristic helps to avoid scan blindness effects.

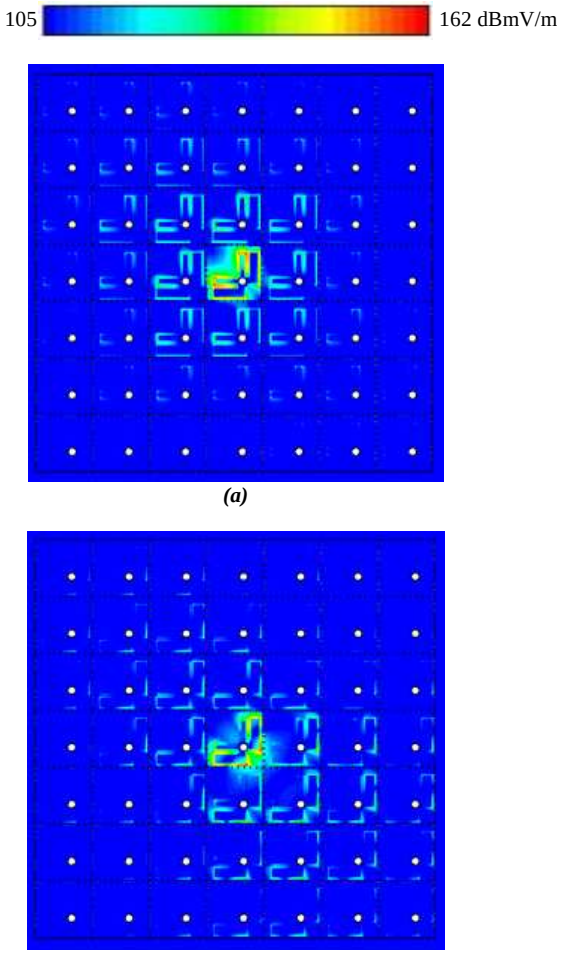

(a)

(b)

Fig. 7. Computed field distribution plot with the excitation of the centre element (no: 25) of the planar array. (a)- 9.8 GHz and (b)- 17 GHz. Yellow circles represent feeding pin positions of the array antennas.

TABLE I
OPTIMISED ANTENNA DIMENSIONS

Parameter	Value (mm)
l_1	8.3
l_2	6.6
w_1	1.35
w_2	1.75
d_r	1.9
U_{cell}	10 × 10
t	1.57
ε_r	2.2

III. EXPERIMENTAL VERIFICATION

A. Measurement setup

The fabricated 49-element planar (7 × 7) array, along with its connector assembly, is shown in Fig. 8. The array measures 70 mm × 70 mm. The thickness of the array face, which measures only 1.58 mm ($0.05\lambda_L$), adds to the low-profile dimensions of the array. Due to the small unit-cell dimensions (10 mm × 10 mm), conductive adhesive was used for mounting the SMA connectors of the individual array elements on the ground plane. The DUCAT anechoic chamber at TU-Delft, used for carrying out the measurements, is optimised for measurements in the 4 – 40 GHz range. The experimental setup is shown in Fig. 9. A ridged horn antenna with an operational range of 2 – 20 GHz was used as the reference (REF) transmitter antenna (Fig. 9b). The array under test (AUT) was kept on the pedestal of the turn table, held in place by a custom-made foam support (Fig. 9a). The radiation pattern measurements were carried out by electronically rotating the turn table.

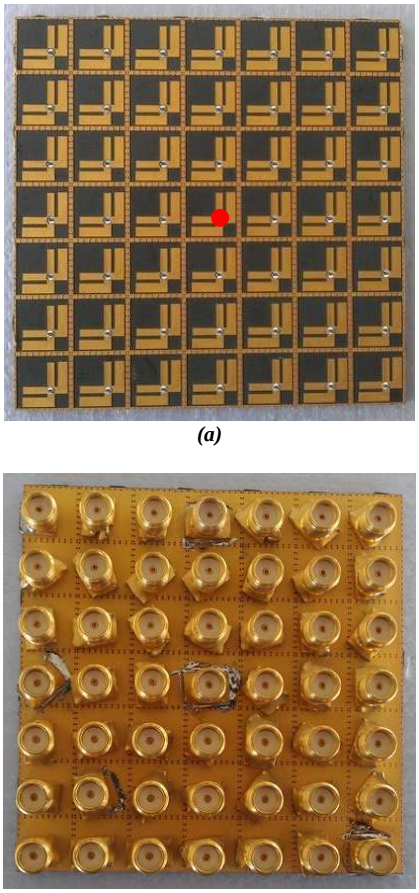

(a)

(b)

Fig. 8. Fabricated dual-band planar array prototype. (a) – Top view and (b) – connector assembly. Red dot – centre element (no: 25).

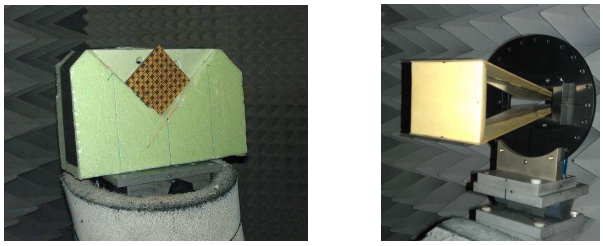

(a) *(b)*

Fig. 9. Anechoic chamber measurement setup. (a) – Array under test (AUT) and (b) – reference ridged horn antenna (REF).

B. *Performance summary*

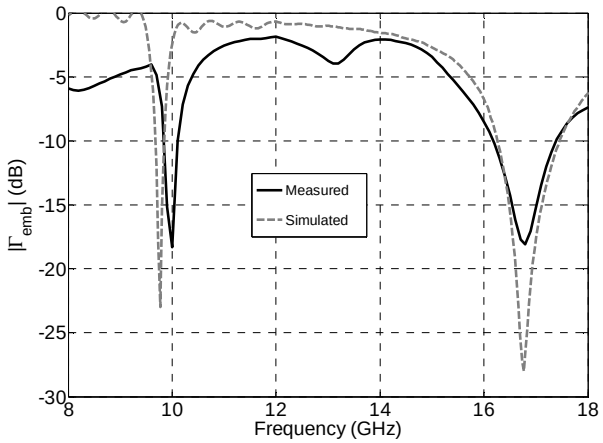

Fig. 10. Measured and simulated embedded reflection coefficient (S_{2525}) of the centre element of the planar (7 × 7) array.

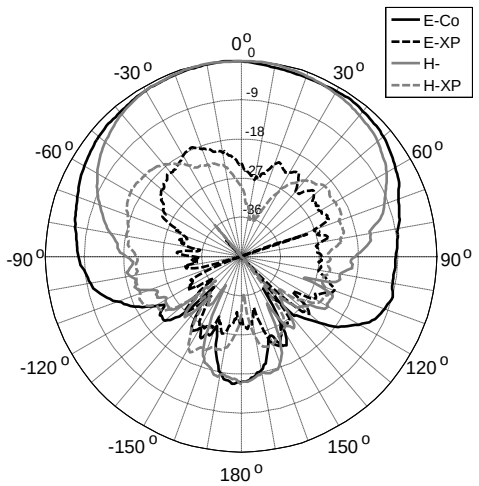

(a)

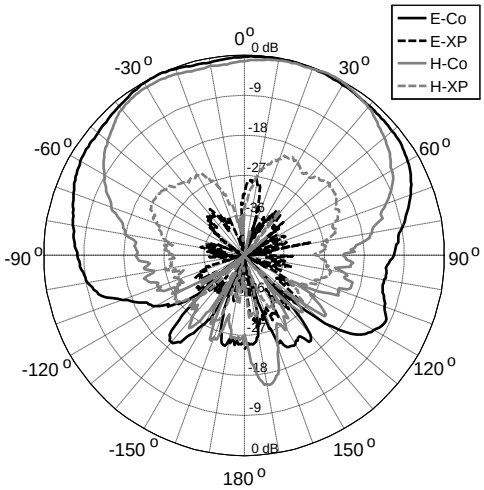

(b)

Fig. 11. Measured embedded radiation patterns of the centre element (no: 25). (a)- 9.9 GHz (f_L) and (b)- 17.1 GHz (f_H).

A comparative plot of the computed and measured embedded reflection coefficient ($|\Gamma_{emb}|$) of the centre-element (no: 25) of the planar array is presented in Fig. 10. The inclusion of the fabrication related constraints and tolerances in the antenna design (such as substrate values, element dimensions and cavity via diameters), as mentioned earlier, has positively aided in achieving this performance conformance. The difference in the band position at the low frequency is mainly attributed to the slight difference in the effective permittivity of the fabricated model due to the adhesive layers, which have higher permittivity (ε_r=3) compared to that of the substrate (ε_r=2.2). Measured bandwidths of 270 MHz (9.81–10.08 GHz) and 1.2 GHz (16.2–17.4 GHz) are achieved at the low and high frequency bands, supporting a maximum frequency ratio of nearly 1.8:1.

Embedded radiation patterns were measured along the principal φ = 45° (H-) and φ = 135° (E-) planes of interest (refer to Fig. 2a for φ-plane marking). To illustrate the broad and consistent radiation patterns supported by the array antenna in both operational bands, the measured embedded patterns of the centre element (no: 25) of the planar array are presented in Fig. 11. It can be inferred (from Fig. 11) that consistent radiation patterns, with cross polarization [18] levels below -16 dB over the entire angular range, are achieved in both operational bands. These broad patterns are vital for achieving wide-angle scanning, the performances of which are presented next.

The scanning performances, based on the measured embedded radiation patterns of the array elements at the low and high frequency bands, are presented in Fig. 12 and Fig. 13 respectively. Grating-lobe-free beam scanning up to a maximum of 60° and 50° are achieved at the low and high frequency bands. The broader beam patterns at the low frequency band (Fig. 12) are primarily due to the small electrical dimensions of the planar array at the respective band. More directive patterns are exhibited at the high frequency band, as a consequence of the large frequency ratio, which in turn results in comparatively larger electrical dimensions of the planar array.

In both the cases, even with a uniformly excited array, the sidelobe levels are maintained below -14 dB for all scanning angles (up to 60° and 50° at the low and high frequency bands). The sidelobe levels can be further reduced by applying an appropriate amplitude taper, if required. The combination of electrically small unit-cell dimensions, which measures only 0.58λ × 0.58λ, at the high frequency band, and broad embedded radiation patterns, enables this excellent wide-angle scanning capability. The demonstrated wide-angle scanning at both the operational bands, even with a large frequency ratio (~1.8:1), and extremely low-profile unit-cell dimensions strongly emphasize the novel characteristics of the proposed dual-band array antenna concept.

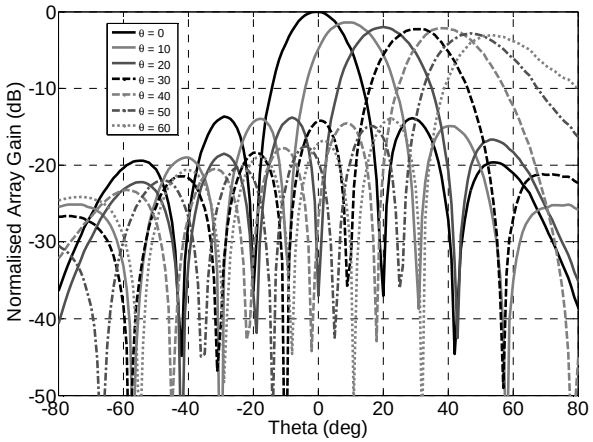

(a)

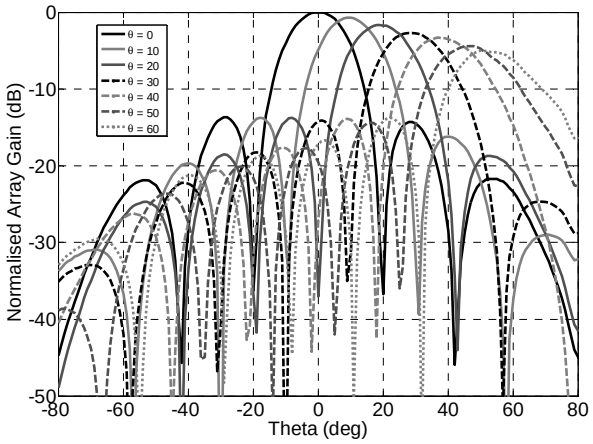

(b)

Fig. 12. Scanning performance of the array at low frequency band of operation (9.9 GHz). (a)– E-plane and (b)– H-plane.

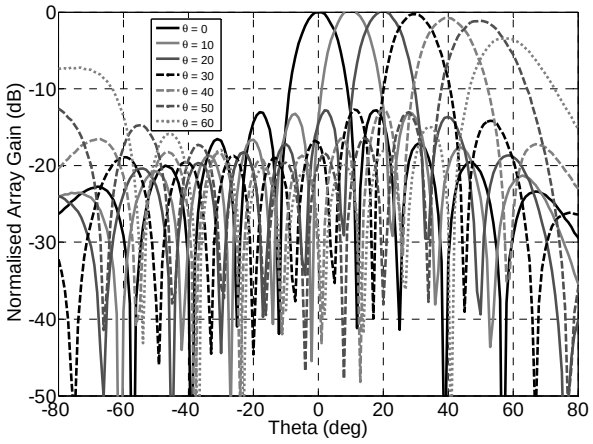

(a)

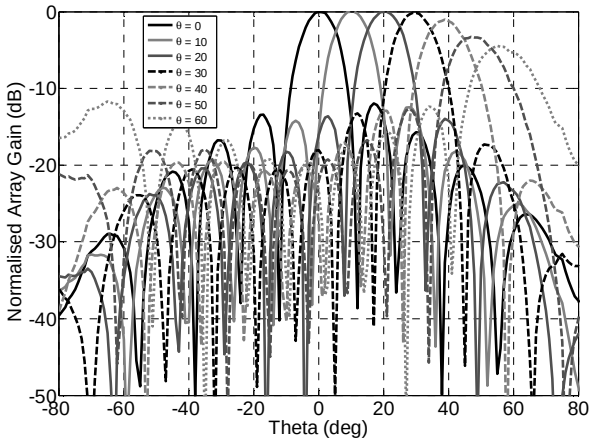

(b)

Fig. 13. Scanning performance of the array at high frequency band of operation (17.1 GHz). (a)– E-plane and (b)– H-plane.

IV. Conclusion

The development and experimental validation of a novel dual-band phased array design, operational in the X/Ku-bands, has been presented. The demonstrated novelties of the dual-band array design include the maintenance of large frequency ratio between operational bands, low levels of coupling, broad and consistent embedded radiation patterns, wide-angle beam scanning and extremely low-profile electrical dimensions of the array antennas. The simple one-layer architecture is another advantage of the antenna design. These aspects represent a strong value addition to the domain of dual-band phased arrays. The proposed dual-band array design might also be attractive for focal-plane arrays, due to its well-separated operational bands and extremely low-profile electrical dimensions. This, to the best of the authors' knowledge, is one of the first successful demonstrations of a dual-band wide-angle scanning phased array with large frequency ratio.

Acknowledgment

The authors wish to thank Pascal Aubry for his help with the demonstrator measurements. The authors thank the reviewers for their constructive comments which helped improve the quality of the manuscript.

References

[1] J. Herd, D. Carlson, S. Duffy, M. Weber, G. Brigham, M. Rachlin, D. Cursio, C. Liss, C. Weigand, "Multifunction Phased Array Radar (MPAR) for aircraft and weather surveillance," *IEEE Radar Conference 2010*, vol., no., pp.945-948, 10-14, May 2010.

[2] A. Ouacha, A. Fredlund, J. Andersson, H. Hindsefelt, V. Rinaldi, C. Scattoni, "SE-IT joint M-AESA program: Overview and status," *Proc. of European Conference on Antennas and Propagation 2010*, vol., no., pp.1-5, 12-16, Apr 2010.

[3] A. Cetronio, M. D'Urso, A. Farina, C. Lanzieri, L. Timmoneri, M. Teglia, "Phased array systems and technologies in SELEX-Sistemi Integrati: State of art and new challenges," *IEEE International Symposium on Phased Array Systems and Technology (ARRAY), 2010*, vol., no., pp.44-49, 12-15 Oct. 2010.

[4] Raytheon Company. “Naval radars: Dual band radars (DBR).” Internet: http://www.raytheon.com/businesses/rids/businesses/scs/navalradars/dbr/index.html. 2012.

[5] N. Riley, D. Riley, Jian-Ming Jin, "Design and modeling of finite and low-profile, ultra-wideband phased-array antennas," *IEEE International Symposium on Phased Array Systems and Technology (ARRAY), 2010*, vol., no., pp.484-491, 12-15 Oct. 2010.

[6] C. T. Rodenbeck, K. Sang-Gyu, Wen-Hua Tu, M. R. Coutant, Seungpyo Hong, Li Mingyi, Kai Chang, "Ultra-wideband low-cost phased-array radars," *IEEE Transactions on Microwave Theory and Techniques*, vol.53, no.12, pp. 3697- 3703, Dec. 2005.

[7] D. Cavallo, A. Neto, G. Gerini, "A 10.5–14.5 GHz wide-scanning connected array of dipoles with common-mode rejection loops to ensure polarization purity," *IEEE Antennas and Propagation Society International Symposium, 2010*, vol., no., pp.1-4, 11-17 July 2010.

[8] K. F. Lee, K. M. Luk, K. M. Mak, S. L. S. Yang, “On the use of u-slots in the designs of dual and triple-band patch antennas,” *IEEE Antennas and Propagations Magazine*, vol.53, no.3, pp.60-74, June 2011.

[9] S. Maci, G.B. Gentili, "Dual-frequency patch antennas," *IEEE Antennas and Propagation Magazine*, vol.39, no.6, pp.13-20, Dec 1997.

[10] M. Veysi, M. Kamyab, A. Jafargholi, “Single-feed dual-band dual-linearly-polarized proximity-coupled patch antenna,” *IEEE Antennas and Propagation Magazine*, vol.53, no.1, pp.90-96, Feb. 2011.

[11] R. D. Bari, T. Brown, S. Gao, M. Notter, D. Hall, C. Underwood, “Dual-polarized printed S-band radar array antenna for spacecraft applications,” *IEEE Antennas and Wireless Propagation Letters*, vol. 10, no., pp. 987 – 990, 2011.

[12] T. Chan, Y. Hwang, “A dual-band microstrip array antenna,” *IEEE Antennas and Propagation Society International Symposium*, 1995, AP-S, Digest, vol.4, pp. 2132-2135, 1995.

[13] K. Jhamb, L. Li, K. Rambabu, “Novel integrated patch antennas with multi-band characteristics,” *IET Microwaves, Antennas and Propagation*, vol 5, no. 12, pp. 1393-1398, September 2011.

[14] A. Thain, G. Peres, A. Hulzinga, H. Schippers, H. Van Gemeren, “A dual-band low profile phased array antenna for civil aviation applications,” *3rd European Conference on Antennas and Propagations, EUCAP*, vol., no., pp.1337-2341, 23-27 March 2009.

[15] A. A. Deshmukh, K. P. Ray, “Multi-band configuration of stub-loaded rectangular microstrip antennas,” *IEEE Antennas and Propagation Magazin*e, vol.52, no.1, pp.89-103, Feb. 2010.

[16] Rogers Corporation. “Product selection guide.” Internet: http://www.rogerscorp.com.

[17] S. E. Valavan, D. Tran, A. G. Yarovoy, “A novel circularly-polarised quad-band patch antenna for satellite applications,” *to be published.*

[18] A. Ludwig, "The definition of cross polarization," *IEEE Transactions on Antennas and Propagation*, vol.21, no.1, pp. 116- 119, Jan 1973.